Structures, Electronic States and Electroluminescent Properties of a Series of Cu^{I} Complexes

Li Yang,[a] Ji-Kang Feng,*[a,b] Ai-Min Ren,[a] Ming Zhang,[c] Yu-Guang Ma,*[c] and Xiao-Dong Liu[b]

Keywords: Copper / Density functional calculations / N ligands / Photoluminescence

A series of new mixed-ligand copper(I) complexes [Cu(NN)-POP]BF_4, where NN = 1,10-phenanthroline (phen; **1a**), 2,9-dimethyl-phen (DMphen; **1b**), 4,7-diphenyl-phen (DPpehn; **1c**) and 2,2′-bipyridine (bpy; **2a**), have been synthesized. Density functional theory (DFT) was applied to study the ground- and excited-state properties of these copper(I) complexes. The electronic structure variation is obtained by changing the substituted positions on the phenanthroline ligand. A time-dependent-DFT approach (TDDFT) was used to interpret the absorption and emission spectra in this system based on the optimized geometries at the B3LYP/LANL2DZ and CIS/LANL2DZ levels of theory, respectively. The results show that the lowest-energy excitations of all complexes are dominated by $d\pi(Cu)\rightarrow\pi^*$(phen) or bpy (MLCT) excitations. In particular, the lowest triplet state (T_1) corresponds to an excitation from the HOMO to the LUMO in all considered complexes, and emissions occur from T_1, assigned to ^{3}MLCT. Steric effects exerted by the pendent groups at the 2- and 9-positions of the phenanthroline ligands increase the HOMO–LUMO gaps and thus lead to a blue-shift of both absorption and emission spectra and effectively prevent structural relaxation in the MLCT state, which may narrow the energy gap between the excited and ground states and therefore increase nonradiative decay.

Introduction

The development of practical components for chemical sensors,[1,2] display devices,[3,4] probes of biological systems,[5,6] phototherapy,[7] and solar-energy conversion[8] schemes has fuelled interest in complexes of polypyridine and phenanthroline ligands with transition metals, especially heavy metal ions such as ruthenium(II) or rhenium(I).[9] At the same time, the strongly appealing possibility of using cheap copper(I) complexes for replacing the more expensive compounds based on ruthenium(II) or other metal ions, along with the need for a deeper understanding of the correlation between structural processes and photophysical properties, have pushed a continuous progress in the design of photoluminescent Cu^{I} complexes. However, the emission signals from charge-transfer (CT) excited states of copper(I) complexes are typically weak and short-lived[10–12] because the lowest energy CT state of a d^{10} system involves excitation from a metal–ligand $d\sigma^*$ orbital.[10] An important consequence is that the excited state typically prefers a tetragonally flattened geometry whereas the ground state usually adopts a more tetrahedral-like coordination geometry appropriate for a closed-shell ion.[10,13] Aside from reducing the energy content, the geometric relaxation that occurs in the excited state facilitates relaxation back to the ground state.[14,15] Moreover, donor media also tend to quench the lifetime. Blaskie and McMillin first reported this type of exciplex quenching, and by now, many other studies have confirmed the mechanism. Mixed-ligand systems involving triphenylphosphane initially looked promising because they exhibit long lifetimes in the solid state and frozen solution.[16,17] However, detailed studies of $[Cu(phen)(PPh_3)_2]^+$ (phen = 1,10-phenanthroline) have shown that it is virtually nonemissive in methanol, while $[Cu(dmp)(PPh_3)_2]^+$ (dmp = 2,9-dimethyl-1,10-phenanthroline) has a lifetime of 330 ns in deoxygenated solution.[16] However, even with two bulky triphenylphosphanes and a sterically active dmp ligand in the coordination sphere, temperature-dependent emission studies suggest that photoexcited $[Cu(dmp)(PPh_3)_2]^+$ is still subject to exciplex quenching in methanol.[18] An obvious possibility was that incorporation of a chelating phosphane might suppress ligand dissociation.[19] In this context, a series of new mixed-ligand copper(I) polypyridine and phenanthroline complexes such as $[Cu(NN)(POP)]^+$ [POP = bis-{2-(diphenylphosphanyl)phenyl} ether] that are vastly superior luminophores have been synthesized. It is found that solvent-induced exciplex quenching is relatively

[a] State Key Laboratory of Theoretical and Computational Chemistry, Institute of Theoretical Chemstry, Jilin University, Changchun 130023, P. R. China
Fax: +86-431-894-5942
E-mail: Jikangf@yahoo.com
[b] The college of Chemistry, Jilin University, Changchun 130023, P. R. China
[c] Key Lab for Supramolecular Structure and Materials of the Ministry of Education, Jilin University, Changchun 130023, P. R. China

inefficient for the CT excited state of this POP system. On the other hand, introduction of sterically demanding ligands can impede geometric relaxation as well as solvent attack. Here, steric effects exerted by pendent groups at the 2,9- and different buttressing groups at the 3,7-phenanthroline positions cooperate to effectively block the excited state close to the ground-state geometry. A further approach for blocking structural rearrangements at the excited state is based on the use of aryl groups appended to the phen unit. The metal-to-ligand charge transfer (MLCT) excited states of cuprous diimine compounds are often luminescent and play important roles in photoinduced electron and energy transfer.

Reaction of $[Cu(NCCH_3)_4]BF_4$ with POP and a polypyridine or phenanthroline ligand gives good yields of the copper(I) complexes $[Cu(NN)POP]BF_4$, where NN = 2,2′-bipyridine and substituted bipyridine ligands or phenanthroline and substituted phenanthroline ligands. The emission from $[Cu(NN)(POP)]^+$ is very similar to that reported for the $[Cu(NN)(PPh_3)_2]^+$ system in room temperature DCM solution.[18] Whereas the photophysical properties of $[Cu(NN)(POP)]^+$ systems vary dramatically with the steric requirements of the NN ligand, the steric influence of the alkyl substituents is also evident in the electrochemistry.

In contrast to experimental studies, so far very little theoretical work is available on Cu^I systems. Despite this fact, density functional theory (DFT) has been successful at providing a means to evaluate a variety of ground-state properties with an accuracy close to that of post-HF methods.[20,21] As a consequence, time-dependent density functional theory (TDDFT) has emerged as an accurate method for the calculation of excited state properties of molecules.[22,23] Because of the low computational costs and complexity, TDDFT is applicable to fairly large systems (for recent applications see, for example, refs.[24,25]) for which traditional wavefunction-based methods are not feasible. Only very recently, a DFT study of the Cu^I systems limited to geometry optimization of the molecular structure and the electronic structure, but no excited geometry optimization of the molecular structure and emission spectra, have been performed.[26,27] On the other hand, a theoretical investigation has been performed at the complete DFT level for Ru^{II} complexes such as $[Ru(bpy)_3]^{2+}$ and [Ru(4,4′-COOH-2,2′-bpy)$(NCS)_2$], but there is still no excited state study.[28] In fact, until now the standard method for calculating excited state equilibrium properties of larger molecules is the configuration interaction singles (CIS) method. However, the calculation of excited-state properties typically requires significantly more computational effort than is needed for the ground states and is dramatically constrained by the size of the molecules.

In this paper we report on a series of new copper(I) mixed-ligand complexes, as well as the structures of complexes $[Cu(NN)POP]BF_4$, where NN = 1,10-phenanthroline (phen; **1a**), 2,9-dimethyl-phen (DMphen; **1b**), 4,7-diphenyl-phen (DPpehn; **1c**) and 2,2′-bipyridine (bpy; **2a**; Figure 1). Furthermore, we present a theoretical and experimental investigation of this series of copper(I) mixed-ligand complexes, including DFT calculations of the structural and electronic properties, as well as a TDDFT study of the main features of the near UV/Vis spectra and, more importantly, the excited state and photoluminescence character. The effect of variation of the substituted positions on the lowest-energy excited states of the complexes has been assessed by calculating their electronic structures and excitation energy. We show that with a reasonable computational effort TDDFT well reproduces the spectroscopic properties of the copper(I) mixed-ligand systems, suggesting that this approach could be used to provide insight into the design of new and more-efficient photoluminescent Cu^I complexes.

Results and Discussion

Molecular Structure and X-ray Single-Crystal Diffraction

The molecular structure of the Cu^I complexes was determined by X-ray single-crystal diffraction. The calculated

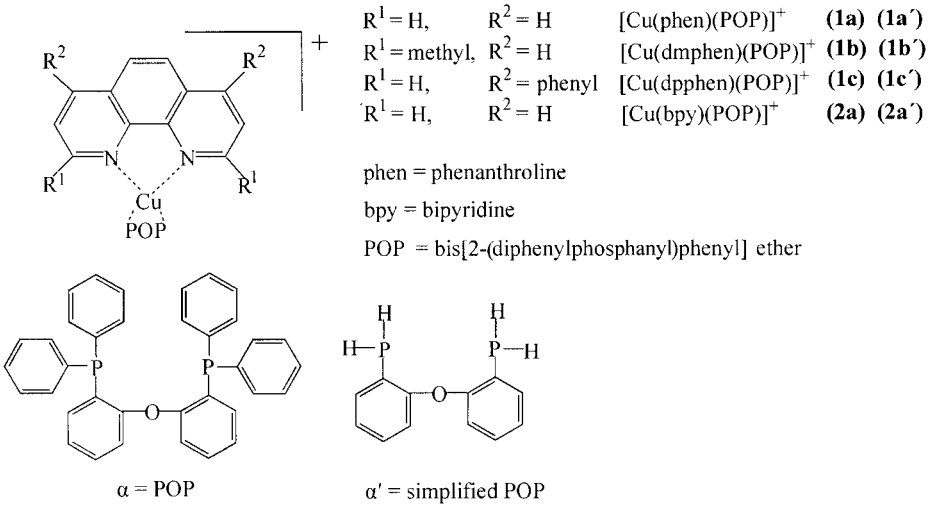

Figure 1. Schematic structures of complexes **1a**–**1c** and **2a** with the POP (α) ligand and **1a′**–**1c′** and **2a′** with the simplified POP ligand (α′).

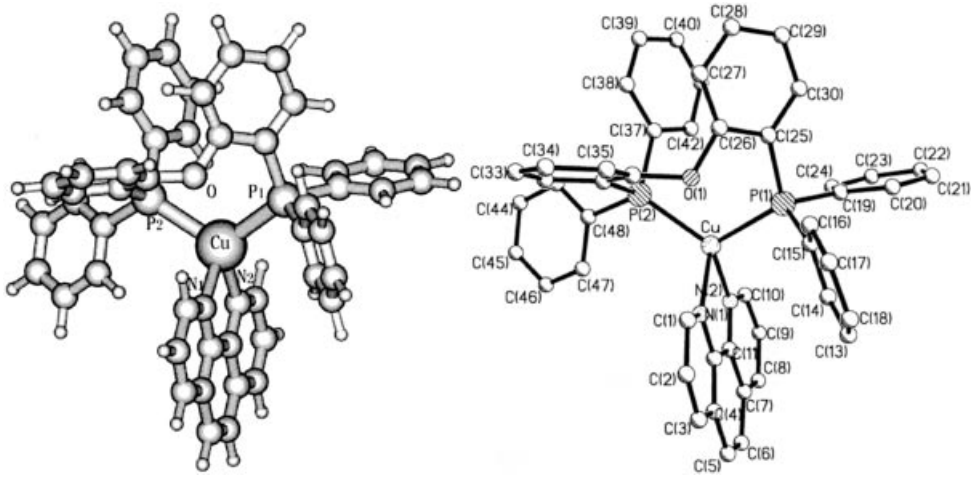

Figure 2. Calculated (left) and crystal (right) structures of complex **1a**.

and crystal structures of complex **1a** are shown in Figure 2, which shows that the calculated structure agrees well with experimental one. Both structures reveal a distorted tetrahedral coordination environment about Cu^{I} with P–Cu–P and N–Cu–N bond angles of 113.52° and 80.88°, respectively. The ether oxygen atom of POP is at a nonbonding distance (>3.1 Å) to the metal center. The resulting eight-membered ···C–C–P–Cu–P–C–C–O··· rings assume a tublike conformation in the solid state, with a dihedral angle between the phenyl rings of 77.9° for complex **1a**. All three $[Cu(NN)(POP)]^{+}$ complexes exhibit similar structures.

The only complex for which a significant intermolecular interaction is present in the solid state is compound **1a**, where the phen ligands of the pairs of symmetry-related cations partially overlay one another (Figure 3). The components of this pair are related to one another through a center of inversion that is located between the phen rings; the closest intermolecular C···C and C···N contacts are in the range 3.59–3.64 Å.

Selected bond lengths and angles for compounds **1a**–**1c** and **2a** are listed in Table 1. The introduction of POP suppresses ligand dissociation and unexpectedly makes the solvent-induced exciplex quenching relatively inefficient for the CT excited state. However, since these POP ligands have little influence on the study of UV/Vis spectra, the excited state, and photoluminescence character, the four phenyls bound to phosphorus but not to oxygen were substituted by hydrogen in order to simplify th calculation, as shown in Figure 1. This simplification has little effect on the molecular structure. In fact, the differences of bond lengths and angles between calculated and experimental structures are within 0.4 Å and 5°, respectively, in all cases. For **1a**, for example, the Cu–N(1) bond length and the N(1)–Cu–N(2) angle differ by 0.04 Å and 0.1°, respectively, from the experimental data; these values are 0.01 Å and 0.8° for **1a**′. The largest difference occurs for P(1)–Cu–P (2), which decreases by nearly 8° compared with the experimental value, although this does not influence the theoretical study of absorption and emission properties. Interestingly, a comparison of the calculated values of simplified structures shows

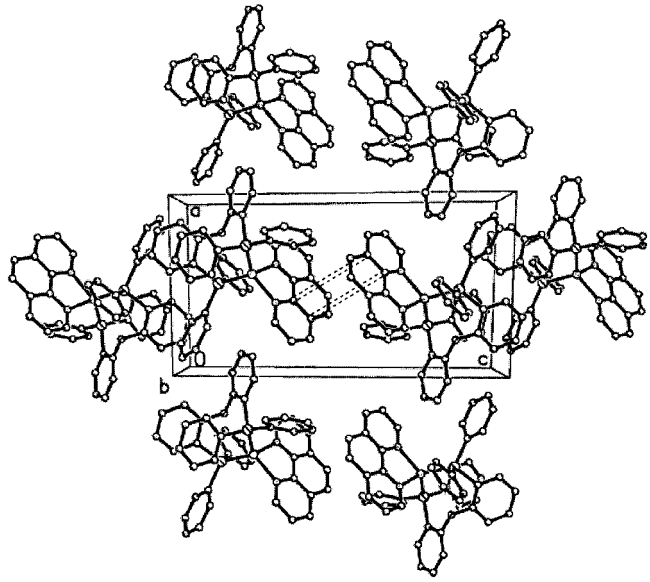

Figure 3. Crystal packing of complex **1a**.

that the Cu–N bond lengths are more strongly influenced than the Cu–P bond lengths by substituents at the 4,6-positions − the latter ones remain nearly equal, whereas the former differ by about 0.02 Å (comparison between **1a**′ and **1c**′). On the contrary, the substituents at the 2,9-positions have less influence on the Cu–N than on the Cu–P bond lengths; the latter differ by about 0.02 Å (comparison between **1a**′ and **1b**′). These structural characteristic should have significant effects on the orbital energy, absorption spectra, and luminescent properties.

A summary of the crystal data for complexes **1a**, **1b**, and **2a** can be found in the Experimental Section. These results indicate that the single crystal has good morphological, structural, and molecular stabilities.

Electronic Structure

Since the observed differences in the chemical and physical properties of the complexes rely primarily on the

Table 1. Experimental and calculated structure parameters for complexes **1a**–**1c** and **2a**.

	1a				**1b**			**1c**		**2a**	
	Exp.[a]	Exp.[b]	Calcd.[c]	Calcd.[d]	Exp.[a]	Exp.[b]	Calcd.[d]	Calcd.[d]	Exp.[a]	Calcd.[c]	Calcd.[d]
Cu–N(1)	2.078	2.071	2.113	2.102	2.098	2.104	2.102	2.084	2.085	2.102	2.090
Cu–N(2)	2.073	2.064	2.108	2.095	2.075	2.084	2.098	2.089	2.034	2.101	2.079
Cu–P(1)	2.271	2.261	2.402	2.427	2.285	2.273	2.441	2.426	2.245	2.423	2.423
Cu–P(2)	2.235	2.231	2.42	2.414	2.228	2.269	2.421	2.417	2.232	2.402	2.413
Cu···O		3.205	3.164	3.386		3.151	3.444	3.415		3.092	3.347
P(1)–Cu–P(2)	113.52	110.81	114.16	106.46	117.04	116.44	106.58	106.61	111.97	113.47	106.20
N(1)–Cu–N(2)	80.88	80.83	80.97	81.75	81.39	80.88	82.23	81.20	80.13	79.65	80.74
N(1)–Cu–P(1)	103.80		119.38	120.25	108.88		119.28	119.10	123.58	120.06	121.80
N(1)–Cu–P(2)	113.53		116.17	117.89	119.55		115.40	118.42	114.72	111.14	113.74
N(2)–Cu–P(1)	113.50		110.37	114.54	118.84		116.28	114.63	114.73	116.54	121.80
N(2)–Cu–P(2)	124.88		110.18	114.59	105.40		116.11	115.53	109.40	110.64	119.70

[a] Our experimental structure. [b] See ref.[30] [c] Structure with POP. [d] Simplified structure.

changes in the ground-state electronic structure, before dealing with the excited states, we will discuss in detail the ground-state electronic structure of these complexes with a special emphasis on the frontier orbital components and HOMO–LUMO energy gaps. The assignment of the nature of each MO was made on the basis of its composition [see Tables 2 and 3 in which only the most important occupied and virtual (unoccupied) orbitals are listed] and by visual inspection of its three-dimensional representation (see Figures 4 and 5, which show complexes **1a′** and **1b′** as examples, respectively). The atomic orbital contributions for each complex, expressed in percent, are given in Tables 2 and 3. Percent contributions were calculated from Equation (1), where n is the atomic orbital coefficient and $\sum n^2$ is the sum of the squares of all atomic orbital coefficients in a specific molecular orbital.

$$[n^2/\sum n^2] \times 100 = \% \text{ contribution} \quad (1)$$

Every complex is divided into four parts: the metal Cu, pyridine ligand, simplified POP, and different substituents R. Each part of the percent contributions are the sum of the atomic orbital coefficient squares.

In general, for all the investigated complexes, their occupied orbital compositions are perturbed by different substitution positions, but the relative ordering and characters are not changed, as shown in Tables 2 and 3: the two highest occupied orbitals have predominant metal Cu d character (54%, 62%, 53% and 63% in HOMO and 64%, 56%, 59% and 54% in HOMO–1 for **1a′**, **1b′**, **1c′**, and **2a′**, respectively), admixed with some contributions from the phen (bpy) ligand and POP. The HOMO–3 orbital for substituted complexes **1b′** and **1c′** also features roughly metallic antibonding character (60% and 44%, respectively), but for unsubstituted complexes **1a′** and **2a′** the HOMO–3 orbitals are predominantly delocalized on the POP ligand (57% and 65%, respectively), although significant metal contributions (36% and 30%, respectively) remain. Some

Table 2. G03/B3LYP calculated one-electron energy and percentage composition of selected frontier MOs of **1a′** and **1b′** expressed in terms of component fragments.[a]

MO	Energy [eV]	Character **1a′**	phen	Cu	POP	MO	Energy [eV]	Character	phen **1b′**	Cu	POP	Me
115(V)	–2.85	phen	96	1	3	122(V)	–2.84	POP	2	2	94	2
113(V)	–3.00	POP	1	2	97	121(V)	–3.02	POP	2	2	95	1
112(V)	–3.25	POP	2	2	96	119(V)	–3.38	phen	82	2	13	1
111(V)	–3.40	POP	2	2	96	118(V)	–3.41	POP	9	2	88	1
110(V)	–3.64	phen	97	1	2	117(V)	–4.51	phen	97	0	0	3
109(V)	–4.83	phen	99	0	1	**116(V)**	**–4.71**	**phen**	**95**	**2**	**3**	**0**
108(V)	**–4.94**	**phen**	**96**	**2**	**2**	**115(O)**	**–8.58**	**Cu**	**23**	**62**	**14**	**1**
107(O)	**–8.67**	**Cu**	**14**	**54**	**32**	114(O)	–8.64	Cu	15	56	28	1
106(O)	–8.72	Cu	22	64	14	113(O)	–9.00	Cu	11	60	28	1
105(O)	–9.06	POP+Cu	7	36	57	112(O)	–9.12	POP	4	14	82	0
104(O)	–9.13	POP+Cu	6	42	52	110(O)	–9.51	Cu	25	69	5	1
103(O)	–9.57	POP	23	7	70	107(O)	–9.75	POP+phen	37	21	40	2
102(O)	–9.63	Cu	21	72	7	106(O)	–9.76	POP+phen	33	26	39	2
101(O)	–9.65	phen+POP	44	15	41	103(O)	–11.18	phen	89	5	3	3
97(O)	–10.06	phen	86	13	1							
Energy gap (ΔE) = 3.73 eV (HOMO–LUMO)						**Energy gap (ΔE) = 3.87 eV** (HOMO–LUMO)						

[a] HOMO and LUMO orbitals are shown in bold.

Table 3. G03/B3LYP calculated one-electron energy and percentage composition of selected frontier MOs of **1c′** and **2a′** expressed in terms of composing fragments[a].

MO	Energy [eV]	Character	phen **1c′**	Cu	POP	Me	MO	Energy [eV]	Character **2a′**	phen	Cu	POP
153(V)	–3.04	phen	60	0	2	38	109(V)	–2.74	bpy	94	0	6
152(V)	–3.12	POP	2	2	96	0	108(V)	–2.90	POP	5	5	91
150(V)	–3.42	phen	96	1	3	0	107(V)	–3.06	POP	1	2	97
149(V)	–4.57	phen	91	0	0	9	106(V)	–3.31	POP	1	2	97
148(V)	**–4.66**	**phen**	**88**	**2**	**2**	**8**	105(V)	–3.45	POP	1	2	97
147(O)	**–8.40**	**Cu**	**21**	**53**	**22**	**4**	104(V)	–3.92	bpy	99	0	1
146(O)	–8.42	Cu	24	59	14	3	103(V)	–4.21	bpy	98	1	1
144(O)	–8.94	Cu	18	44	24	14	**102(V)**	**–5.00**	**bpy**	**96**	**2**	**2**
143(O)	–9.00	POP	9	12	67	11	**101(O)**	**–8.67**	**Cu**	**26**	**63**	**11**
142(O)	–9.03	ph	25	11	3	60	100(O)	–8.75	Cu	9	54	37
141(O)	–9.23	ph	3	0	0	97	99(O)	–9.13	POP	5	30	65
140(O)	–9.24	ph	3	0	0	97	98(O)	–9.18	Cu+POP	7	48	46
136(O)	–9.56	phen+ph	52	1	14	34	97(O)	–9.64	POP	4	23	73
135(O)	–9.61	POP	9	17	71	3	96(O)	–9.69	Cu	13	68	19
134(O)	–9.76	POP	1	14	85	0	93(O)	–9.93	phen	81	16	3
Energy gap(ΔE) = 3.74 eV (HOMO–LUMO)							**Energy gap(ΔE) = 3.67 eV** (HOMO–LUMO)					

[a] HOMO and LUMO orbitals are shown in bold.

lower-energy occupied MOs still have significant metal character, but the contributions from phen (bpy) and POP increase. In contrast, the two lowest unoccupied orbitals LUMO and LUMO+1 in each complex are essentially π*-orbitals localized on the phen or bpy moieties (over 90%). LUMO+2 is calculated to have dominant ligand phen or bpy π* character in each complex except for **1b′**, where it is POP-centered (88%). As shown in Tables 2 and 3 higher virtual orbitals are mainly delocalized over the bpy, phen, or POP ligands.

However, comparing **1a′**, **1b′**, and **1c′**, it can be found that there is a greater effect when substituted in the 2,9-phenanthroline positions than in the 4,7-phenanthroline positions. Firstly, the energy gaps (HOMO–LUMO) of **1a′** (3.73 eV) and **1c′** (3.74 eV) are close in energy, and are lower in energy than in **1b′** (3.87 eV). Secondly, the copper d-orbital character in the HOMOs are similar in **1a′** (54%) and **1c′**(53%) and are about 10% lower than that in **1b′** (62%). We interpret this different behavior in terms of structural factors, and suggest that substituents in the 2,9-

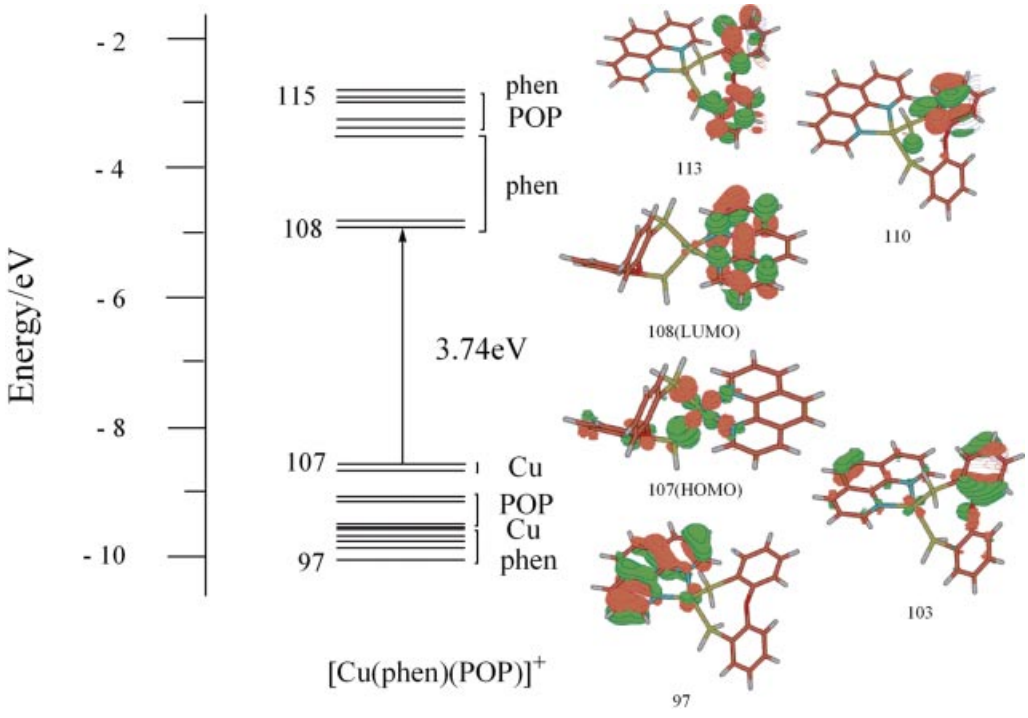

Figure 4. Energy-level diagram of the frontier molecular orbitals together with representative three-dimensional MO plots calculated at the B3LYP/LanL2DZ level for **1a′**. Labels on the right denote the dominant moiety contributing to each molecular orbital. For clarity, only a few of the molecular orbitals are numbered.

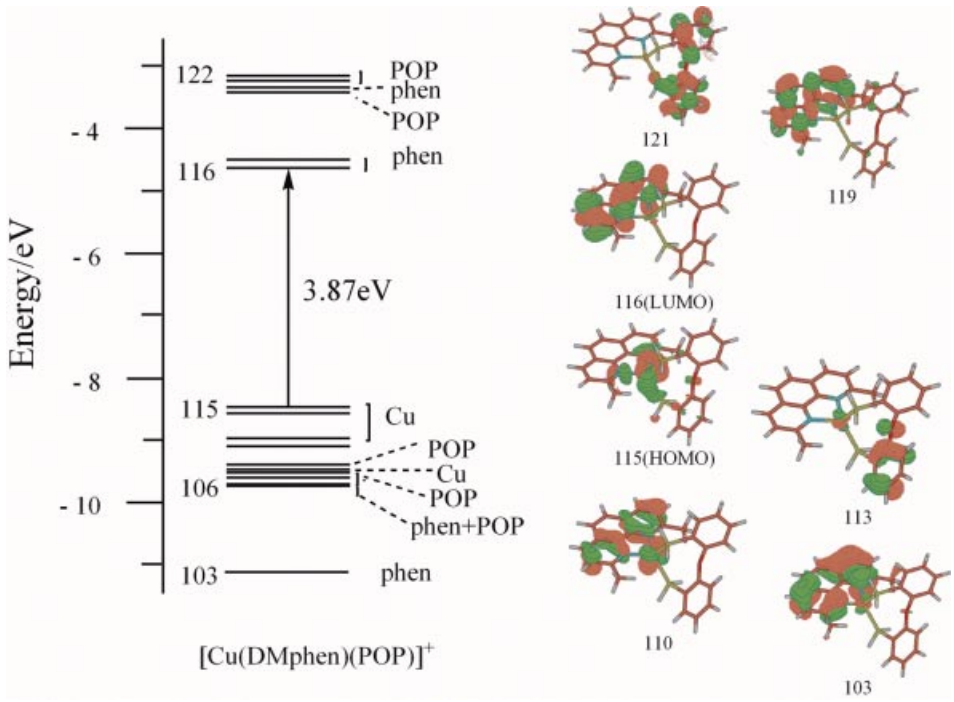

Figure 5. Energy-level diagram of the frontier molecular orbitals together with representative three-dimensional MO plots calculated at the B3LYP/LanL2DZ level for **1b′**. Labels on the left denote the dominant moiety contributing to each molecular orbital. For clarity, only a few of the molecular orbitals are numbered.

phenanthroline positions are optimal to prevent significant ground-state distortions.

The LUMOs of **1a′** and **2a′**, as has already been indicated, are characteristic ofr the two diimines, whereas the valence occupied orbitals exhibit the same character due to the identity of the POP and metal. As from the energetic viewpoint phen and bpy show an almost identical π*-accepting ability (Tables 2 and 3), it is expected that the HOMO–LUMO gap of these complexes will be very similar in energy (differs by 0.06 eV). From the orbital character point of view, the metal's contribution is greater in the latter (about 60%) than in the former (about 50%).

Contour plots of the characteristic occupied and virtual orbitals for molecules **1a′** and **1b′** are depicted in Figures 4 and 5, respectively. In these plots, the metal character is evident in the HOMO, which is an admixture with a phosphorus contribution from POP and a nitrogen contribution from phen (bpy), while the LUMO is delocalized over the phen ligand. Lower-energy occupied orbitals are mainly located on phen and one of POP phenyls, and the higher-energy virtual orbitals are also composed of phen and phenyls of POP.

Cation and Anion Properties

Additional information derived from our calculations provides insight into the interrelationship of structure and electronic behavior, in particular the response of the molecule to the formation of a hole or the addition of an electron. Table 4 contains the ionization potentials (IPs), electron affinities (EAs), and spin density. The vertical IP is obtained by differences in the total self-consistent energies of the cation and the neutral molecule based on the optimized neutral ground-state geometry, as is the EA. In all cases, the energy required to create a hole is about 10 eV and the energy cost to accept an electron is about 3 eV. As shown in Table 4, the cationic spin density for each complex is mainly on the Cu and POP [see Figure 6 (left), which shows **1b′** as an example], which is basically consistent with the orbital character of the HOMO. These all correspond to removal of an electron from the 5d orbital.

Four complexes show relatively weakly bound negative ions, corresponding to the electron affinity. In each complex the unpaired spin density is totally on the phen or bpy ligands [for example, the spin density is mainly on phen in

Table 4. Ionization potentials, electron affinities, and spin densities for the four complexes [eV]. See text for definitions. The IP and EA are vertical values.

		Spin density of cation [%]							Spin density of anion [%]					
	IP [eV]	phen	bpy	Cu	POP	Me	ph	EA [eV]	phen	bpy	Cu	POP	Me	ph
1a′	10.08	10		41	49			2.76	93		2	5		
1b′	9.98	19		33	46	2		3.25	93		1	4	2	
1c′	9.95	23		27	27		23	3.40	93		1	1		7
2a′	10.10		20	41	39			3.47		97	1	2		

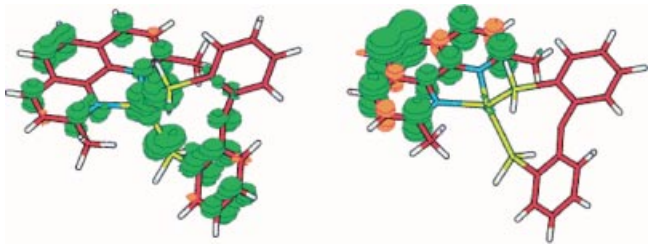

Figure 6. Spin-density surfaces of the cation (left) and the anion (right) for **1b′**.

complex **1b′** as depicted in Figure 6 (right)]. This is consistent with the LUMO being primarily the phen or bpy π*-orbitals.

Absorption Spectra

With the prerequisite ground-state DFT calculation in hand, we proceeded to perform the time-dependent calculation of complexes **1a′** to **2a′** to find the characters and energies of their low-lying singlet and triplet excited states at the TDDFT//B3LYP/LANL2DZ level of theory. Selected low lying singlet and triplet excited states together with their vertical excitation energies and oscillator strengths for **1a′**–**1c′** and **2a′** are displayed in Tables 5, 6, 7, and 8, respectively.

An experimentally used model of an excited state corresponds to the excitation of an electron from an occupied to a virtual MO (i.e., a one-electron picture). However, the excited states calculated herein demonstrate that excited-state electronic structures are best described in terms of multiconfigurations, wherein a linear combination of several occupied-to-virtual MO excitations comprises a given optical transition. Assignment of the character of each excited state was based on the compositions of the occupied and virtual MOs of the dominant configuration(s) for that excited state. Excited states that arise from transitions between orbitals that are located on different moieties were classified as charge transfer (CT) excited states. Those from π-occupied to π-virtual orbitals located on the same ligand were described as π-π* states (IL), but those from orbitals on different ligands were described as ligand-to-ligand charge transfer (LLCT) states. Metal-to-ligand charge transfer (MLCT) states involve transitions from the metal atom to ligand-centered orbitals. For the majority of the excited states under investigation, most of the significant excited states exhibit mixed character as they consist of more than one transition. For example, S_{11} in **1a′** consists of two transitions of 102→109 (45%) and 103→108 (31%). The former transition is from orbital 102, which has mainly metal Cu character, to orbital 109, which is located on phen, and is thus assigned as MLCT, whereas the latter one is from 103(POP) to 108 (phen) and is denoted as LLCT. S_{11} therefore has a mixed character between MLCT and LLCT.

Table 5. Selected TDDFT calculated excitation energies and compositions of the lowest lying singlet and triplet excited states for complex **1a′**.

States	Compositions	ΔE [eV]/$\lambda_{calcd.}$ [nm]	f	$\lambda_{exp.}$ [nm]	Character
		Singlets (**1a′**)			
1	106→108 (55%)	2.81/441	0.0002		MLCT
	107→108 (42%)				MLCT
3	107→108 (53%)	3.19/389	0.1178	391	MLCT
	106→108 (41%)				MLCT
11	102→109 (45%)	4.01/309	0.0148		MLCT
	103→108 (31%)				LLCT
13	102→109 (43%)	4.20/295	0.0134		MLCT
	97→109 (29%)				IL
19	107→110 (50%)	4.45/279	0.0723	269	MLCT
	106→110 (41%)				MLCT
26	107→110 (49%)	4.79/259	0.0518		MLCT
	106→110 (23%)				MLCT
30	105→111 (33%)	4.97/249	0.0582		MLCT + IL
	107→115 (20%)				MLCT
33	107→113 (49%)	5.04/246	0.0391		MLCT
	105→111 (28%)				LLCT + MLCT
		Triplets (**1a′**)			
1	106→108 (55%)	2.64/469	0.0000		MLCT
	107→108 (44%)				MLCT
2	106→108 (55%)	2.81/441	0.0000		MLCT
	107→108 (42%)				MLCT
3	107→108 (53%)	2.82/440	0.0000		MLCT
	106→108 (43%)				MLCT
4	106→109 (41%)	2.87/432	0.0000		MLCT
	101→109 (34%)				LLCT + IL
5	106→109 (56%)	2.99/413	0.0000		MLCT
	107→109 (38%)				MLCT

Table 6. Selected TDDFT calculated excitation energies and compositions of the lowest lying singlet and triplet excited states for complex **1b′**.

States	Compositions	ΔE [eV]/$\lambda_{calcd.}$ [nm]	f	$\lambda_{exp.}$ [nm]	Character
		Singlets (**1b′**)			
1	115→116(62%)	2.95/420	0.0004		MLCT
3	114→116(60%)	3.32/373	0.1016	383[26]	MLCT
5	114→117(62%)	3.53/352	0.0126		MLCT
14	110→117(49%)	4.37/284	0.0164		MLCT
	115→119 (31%)				MLCT
17	115→118 (63%)	4.53/274	0.0236		MLCT
19	114→119 (41%)	4.60/269	0.0622		MLCT
	107→116 (27%)				LLCT + IL
20	106→116 (41%)	4.61/268	0.0233		LLCT + IL
	107→116 (40%)				LLCT + IL
34	114→121 (49%)	5.00/248	0.0430		MLCT
	112→118 (20%)				IL
		Triplets (**1b′**)			
1	115→116(64%)	2.80/443	0.0000		MLCT
2	111→117(53%)	2.91/426	0.0000		IL
	114→117(35%)				MLCT
3	114→116(62%)	2.96/418	0.0000		MLCT
4	115→117(58%)	3.21/387	0.0000		MLCT
	114→117(31%)				MLCT
5	113→116(62%)	3.38/366	0.0000		MLCT

Table 7. Selected TDDFT calculated excitation energies and compositions of the lowest lying singlet and triplet excited states for complex **1c′**.

States	Compositions	ΔE [eV]/$\lambda_{calcd.}$ [nm]	f	$\lambda_{exp.}$ [nm]	Character
		Singlets (**1c′**)			
1	146→148 (52%)	2.83/438	0.0004		MLCT
	147→148(46%)				MLCT
3	147→148(50%)	3.20/387	0.2139	400	MLCT
	146→148 (44%)				MLCT
4	147→149(50%)	3.30/376	0.0714		MLCT
	146→149 (45%)				MLCT
9	144→149(51%)	3.84/323	0.2594	290	LLCT + MLCT
	143→149 (24%)				
12	142→149(57%)	3.96/313	0.2429		LLCT + MLCT
	143→149 (17%)				
22	136→148(45%)	4.30/288	0.0326		IL
	146→150 (28%)				MLCT
24	136→148(40%)	4.42/281	0.0436		IL
	147→150 (37%)				MLCT
33	147→152(42%)	4.69/265	0.0936		MLCT
	147→153 (24%)				MLCT
		Triplets (**1c′**)			
1	147→148(45%)	2.66/466	0.0000		MLCT
	146→148 (41%)				MLCT
2	147→149(35%)	2.67/464	0.0000		MLCT
	146→148 (32%)				MLCT
3	147→148(49%)	2.76/450	0.0000		MLCT
	146→148 (45%)				MLCT
4	146→148(52%)	2.83/438	0.0000		MLCT
	147→148 (46%)				MLCT
5	146→149(52%)	3.00/414	0.0000		MLCT
	147→149 (45%)				MLCT

Furthermore, from Tables 5–8, it can be seen, as in the case of the energy gaps, that the lowest absorption energies in complexes **1a′** (2.81 eV) and **1c′** (2.83 eV) are similar, and both are lower than that of **1b′** (2.95 eV).

The 35 lowest-energy triplet excited states were also calculated by a similar TDDFT methodology. The first five triplet excited states in each complex are listed in Tables 5–8. MLCT, LLCT, and IL excited states are all observed, but

Table 8. Selected TDDFT calculated excitation energies and compositions of the lowest lying singlet and triplet excited states for complex **2a′**.

States	Compositions	ΔE [eV]/$\lambda_{calcd.}$ [nm]	f	$\lambda_{exp.}$ [nm]	Character
		Singlets (**2a′**)			
1	101→102(65%)	2.71/458	0.0003		MLCT
2	100→102 (64%)	3.16/393	0.0975	358	MLCT
9	100→103(65%)	3.92/317	0.0501		MLCT
17	96→103 (46%)	4.55/272	0.0829	285	MLCT
	93→102 (37%)				IL
22	99→104 (49%)	4.81/258	0.0224		LLCT + MLCT
	98→104 (42%)				MLCT
24	96→103 (34%)	4.85/255	0.2055		LLCT + MLCT
	93→102 (32%)				IL
26	101→107 (41%)	4.97/249	0.0367		LLCT + IL
	96→104 (31%)				MLCT
31	99→105 (39%)	5.05/246	0.0305		IL
	100→107 (32%)				MLCT + IL
		Triplets (**2a′**)			
1	101→102 (67%)	2.55/487	0.0000		MLCT
2	100→102 (67%)	2.82/439	0.0000		MLCT
3	98→102 (53%)	3.19/388	0.0000		MLCT + LLCT
	99→102 (43%)				MLCT + LLCT
4	93→102 (51%)	3.25/382	0.0000		IL
	96→102 (44%)				MLCT
5	101→103 (37%)	3.56/348	0.0000		MLCT

most of them are mixed-character excited states, as with the singlets. As expected from Hund's rule, transitions to the triplet states tend to be lower in energy than their corresponding singlets. For example, for complex **1a′** the first triplet vertical transition energy is at 2.64 eV, which is lower than that of the first singlet excited state (2.81 eV), although both represent (predominantly) HOMO and HOMO–1→LUMO transitions. The TDDFT results do not provide information on triplet–singlet absorption intensities since spin-orbit coupling effects are not included in current TDDFT approaches, which is why the oscillator strengths are all zero for triplet excited states. Spin-orbit coupling can, however, mix singlet and triplet states, thereby allowing the latter to acquire intensity in both absorption and emission. A second effect is that the triplet energies are shifted by coupling with higher singlet (or other triplet) states. For third row transition metals one[40] can estimate that the lowest triplet states are lowered by about 0.2–0.3 eV due to interactions with higher states through spin-orbital coupling.

Comparison with Experimental Results

Combined with experimental data gathered over time, computed spectra may provide a reference for monitoring the behavior and possible degradation of the organic material in the device. The results of the TDDFT calculations for all considered complexes have been compared with experimental absorption data (see Tables 5–8 and Figure 7). The spectral assignment is based on a comparison of experimental band maxima with calculated energies of transitions with significant oscillator strengths. However, oscillator strengths should be used rather qualitatively to distinguish allowed transitions from forbidden as very weak transitions to other excited states also occur in the relevant energy regions. Moreover, for the S_1 excited state the calculated spin density of positive and negative ions also has significant reference value for transition assignment. In general, the assignment of the character of each excited state was based on the components of the occupied and virtual MOs (see Tables 2 and 3 and Figures 4 and 5) of the dominant excitation(s) for that excited state.

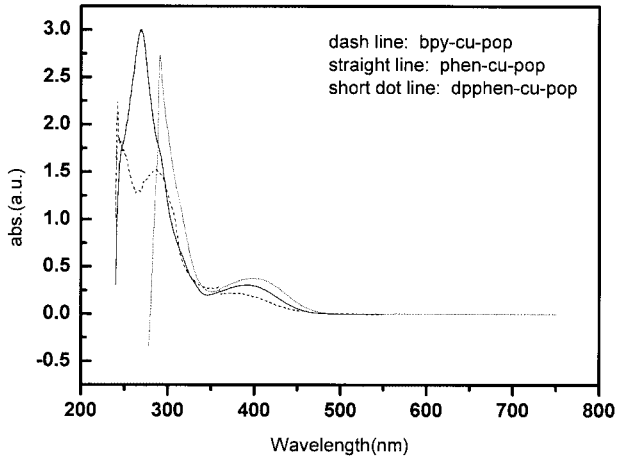

Figure 7. Experimental absorption data of complexes **1a′**, **1c′**, and **2a′** as measured in CH_2Cl_2 solution.

Most of the investigated complexes exhibit two absorption peaks. For complexes **1a′** and **1c′**, the low-energy absorptions are found experimentally at 391 nm and 400 nm,

both of which are similar to the calculated d(Cu)→π*(phen) (MLCT) excitation arising from S_3 at 389 nm (3.19 eV) and 387 nm (3.20 eV). The other intense calculated absorption peak at 269 nm for **1a′**, arising from singlet state S_{19} at 279 nm (4.45 eV), is assigned as having mainly d(Cu)→π*(phen) (MLCT) character. For **1c′** this peak, which corresponds to excited state S_9, features mixed character between d(Cu)→π*(phen) (MLCT) and π→π* (LLCT), and the latter arises from a transition from the POP ligand (HOMO–4) consisting of the π-orbital of phenyl to ligand phen (LUMO).

For complex **1b′**, the low-energy band at 383 nm occurs in the same region as the singlet state S_3 calculated at 373 nm (3.32 eV), which arises from d(Cu)→π*(phen) (MLCT) consisting of HOMO–1→LUMO.

As with complexes **1a′** and **1c′**, the low-energy absorption peak arising from excited state 2 located at 393 nm (3.16 eV) results from d(Cu)→π*(bpy) (MLCT) and agrees with the experimental value of 383 nm in complex **2a′**. The other absorption band labeled as mixed transition of MLCT and π(bpy)→π*(bpy) (IL) is consistent with the experimental band at 285 nm.

It can be seen from the absorption analysis that substitution at the 3,7-phenanthroline positions has less effect than at the 2,9-phenanthroline positions on the absorption bands. for example, the low-energy bands in complexes **1a′** (389 nm) and **1c′** (387 nm) are similar, and are both at longer wavelength than that in **1b′** (373 nm) due to steric effects exerted by the pendent groups at the 2,9-positions. Different ligands bpy and phen have little influence on the absorption spectra. For example, the low-energy absorption band is found at 389 nm in **1a′** and 393 nm in **2a′**.

The good agreement between theory and experiment suggests that the character of the experimental absorption features can be inferred from our calculations. Specifically, the low-energy edge is largely MLCT in nature, whereas the strongest peaks contain significant contributions from LLCT or IL transitions. In fact, it has been shown before that TDDFT frequently underestimates the transition energies of excitations accompanied by a substantial charge density redistribution.[29–33] For example, TDDFT vacuum calculations of the complexes [Ru(X)(R)$(CO)_2$(diimine)] (X = Cl, Br, I, R = X, Me, $SnPh_3$; diimine = bpy or *N*,*N*′-bis-*i*Pr-1,4-diazabutadiene) have predicted that their low-lying MLCT and LLCT transitions occur at energies well below those of the lowest experimental absorption bands.[31–33] Moreover, this method cannot yet be used to study extended systems as it is not infrequent that the optical properties reach saturation already for quite short chain lengths, whereas the orbital energies still continue to change for longer oligomers. It is known that the exchange-correlation (XC) functionals must decrease with increasing chain length; this trend of variation is in line with the expectation that in more extended systems the electronic repulsion is smaller.[34,35] However, in this study the combined use of DFT//B3LYP/LANL2DZ and TDDFT//B3LYP/LANL2DZ provides a reliable theoretical tool to investigate the properties of $[Cu(NN)^2]^+$ systems.

Lowest Triplet States

Because the calculation of excited-state properties typically requires significantly more computational effort than is needed for the ground states, the lowest triplet states, T_1, of only molecules **1a′**, **1b′**, and **2a′** were fully optimized by carrying out ab initio CIS.[36,37] The optimized structure parameters are shown in Table 9.

Table 9. Calculated bond lengths of the lowest triplet state (T_1) for complexes **1a′**, **1b′**, and **2a′**.

	1a′	**1b′**	**2a′**
Cu–N(1)	2.196	2.195	2.172
Cu–N(2)	2.191	2.202	2.170
Cu–P(1)	2.612	2.598	2.633
Cu–P(2)	2.561	2.625	2.576
Cu···O	3.277	3.431	3.415
P(1)–Cu–P (2)	107.13	105.71	105.01
N(1)–Cu–N(2)	77.23	77.72	77.75
N(1)–Cu–P(1)	114.93	118.54	117.98
N(1)–Cu–P(2)	111.50	117.40	114.15
N(2)–Cu–P(1)	123.52	118.28	118.31
N(2)–Cu–P(2)	119.14	117.97	117.98

A general elongation of all the metal–ligand bond lengths between the excited and ground states is observed. For example, in complex **1a′** the Cu–N bond lengths in the triplet state (2.196 and 2.191 Å) are longer than those in the ground state(2.102 and 2.095 Å) by about 0.1 Å, and the distances between the metal atom and carbon atom (Cu–C) are also longer by about 0.2 Å in the triplet state (2.612 and 2.561 Å) than in the ground state (2.427 and 2.414 Å). As far as the angles are concerned, except for N(1)–Cu–N(2), which decreases from 80° to 77°, the other angles vary by 5°.

Emission Spectra

On the basis of the excited triplet-state geometry TDDFT was employed to calculate the emission spectra. The long-lived decay lifetime obtained experimentally revealed that the photoluminescence of the four complexes is

Table 10. Calculated emissions in thin film for complexes **1a′**, **1b′**, and **2a′**.

Complex	Compositions	ΔE [eV]/$\lambda_{calcd.}$ [nm]	$\lambda^{exp.}$ [nm]	Stokes shifts [nm]		Character
				calcd.	exp.	
1a′	107→108 (70%)	2.19/567	561	178	170	MLCT
1b′	115→117 (68%)	2.23/556	524	183	141	MLCT
2a′	101→102 (70%)	2.18/568	560	175	177	MLCT

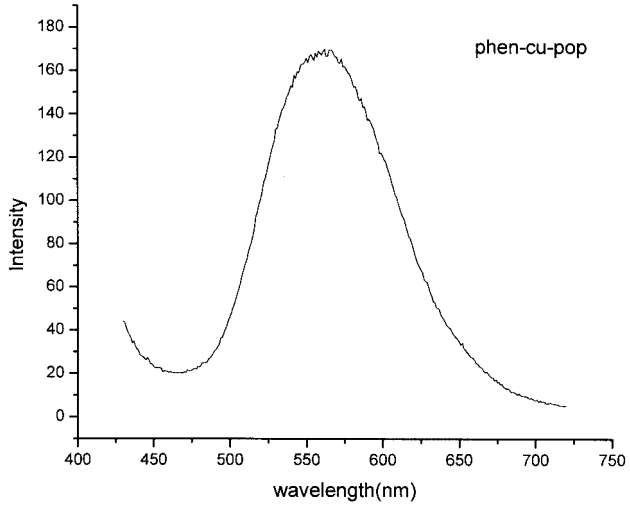

Figure 8. Experimental emission spectra for complex **1a**′ as a thin film.

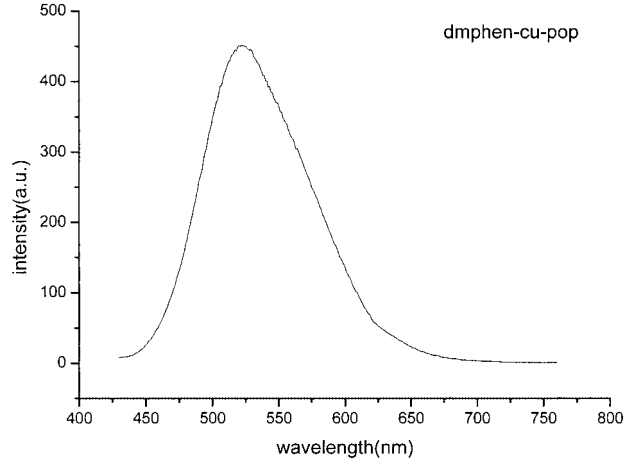

Figure 9. Experimental emission spectra for complex **1b**′ as a thin film.

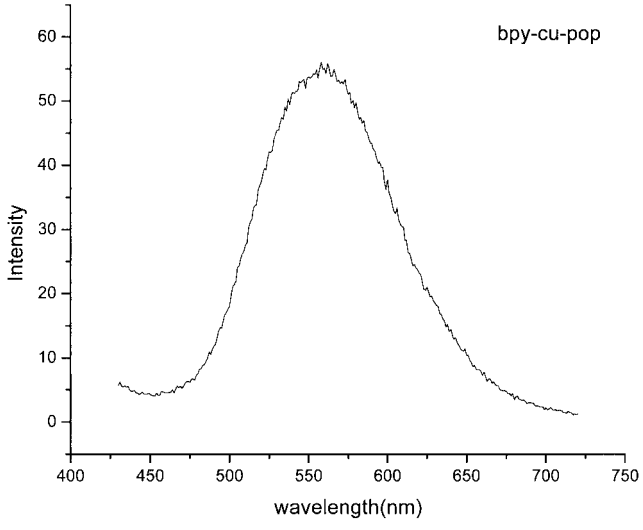

Figure 10. Experimental emission spectra for complex **1c**′ as a thin film.

due to a triplet state transition ($T_1 \rightarrow S_0$) and thus we only optimizes the lowest triplet state (T_1) and calculated the triplet emission spectra. The results of the TDDFT calculations for complexes **1a**′, **1b**′, and **2a**′ are summarized in Table 10, and the experimental emission spectra figures are depicted in Figures 8, 9, and 10 respectively.

The photoluminescence for each complex corresponds to the lowest triplet T_1, which consists of the transition from HOMO to LUMO or LUMO+1, and is thus assigned as having mixed character between MLCT [d(Cu)→π*(phen or bpy)]. The emissions predicted to be at 567, 556, and 568 nm for **1a**′, **1b**′ and **2a**′, respectively, agree well with the experimental values of 561, 524, and 560 nm, and are all assigned to d(Cu)→π*(bpy) (MLCT). It can be seen from these results that all the investigated complexes have large stokes shifts of about 170 nm. Obviously, the change tendency with the different substituted positions of emission is in parallel to that of absorption. In other words, appending groups at 2,9-positions blue-shift the emission spectra due to steric effects.

Conclusions

The ground-state geometries of a series of newly synthesized mixed-ligand, copper(I) polypyridine and phenanthroline complexes such as $[Cu(NN)(POP)]^+$ [POP = bis[2-(diphenylphosphanyl)phenyl] ether] have been calculated at the B3LYP/LANL2DZ level, and the calculated geometrical parameters are in good agreement with the X-ray diffraction experiment results. The electronic structures have been discussed completely. Introduction of groups at the 2,9-positions on the phen ligand lifts the energy gap between the HOMO and the LUMO, and, at the same time, strongly influence the characters of the HOMOs and LUMOs, whereas introduction of groups at the 4,7-positions has little effect on either the energy gap or the character of the frontier orbitals, but makes the orbital characters of the lower occupied and higher unoccupied orbitals change. In addition, there are no pure-metal-character orbitals − the amount of metal 5d character varies from 50% to 70%. Furthermore, substitution at the 2,9-positions makes both the absorption and emission spectra exhibit blue shifts due to steric effects. In all the investigated complexes the lowest-energy absorption and emission are dominant MLCT transitions with some admixture of LLCT transitions. Finally, the results of this work show that careful DFT/TDDFT calculations are capable of accurately describing the spectral features of our investigated complexes, with a quantitative agreement with the experimental data. This suggests that such a theoretical approach may provide useful insights into the design of new and more efficient phosphorescent materials. At the same time, however, it has some drawbacks, especially as it does not consider spin-orbit coupling effects.

Experimental Section

Material and X-ray Diffraction: All complexes, as depicted in Figure 1, were synthesized as described in the literature,[38,39] and then

Table 11. Crystal data and refinement details for complexes **1a**, **1b**, and **2a**.

	1a	**1b**	**2a**
Empirical formula	$C_{50}H_{39}ClCuF_6N_3O_4P_3$	$C_{60}H_{45}Cu_3F_{18}N_6O_3P_3$	$C_{36}H_{38}CuF_2N_{0.67}O_{0.67}P$
Mol. mass	1003.74	1523.55	623.18
Crystal system	triclinic	triclinic	triclinic
Space group	$P\bar{1}$	$P\bar{1}$	$P\bar{1}$
a [Å]	10.8112(6)	15.1463(2)	11.5938(4)
b [Å]	12.3096(7)	18.4820(3)	12.2320(5)
c [Å]	19.5790(12)	18.6955(5)	16.5078(7)
α [°]	80.5030(19)	108.081(3)	79.251(3)
β [°]	86.899(4)	104.560(2)	81.147(2)
γ [°]	72.278(2)	100.7730(11)	72.379(2)
V [Å^3]	2447.9(2)	4611.34(16)	2180.17(15)
Z	2	4	3
F(000)	1026	3060	978
D(calcd.) [mg m^{-3}]	1.362	2.195	1.424
μ [mm^{-1}]	0.661	1.616	0.848
Temp [K]	293(2)	293(2)	293(2)
λ [Å]	0.71073	0.71069	0.71073
2θ range [°]	1.76–27.48	1.21–27.46	1.26–27.37
Final R indices [$I > 2\sigma(I)$]	$R_1 = 0.0704$	$R_1 = 0.0469$	$R_1 = 0.0506$
	$wR_2 = 0.2331$	$wR_2 = 0.1089$	$wR_2 = 0.1468$
R indices (all data)	$R_1 = 0.0864$	$R_1 = 0.1618$	$R_1 = 0.0676$
	$wR_2 = 0.2470$	$wR_2 = 0.1558$	$wR_2 = 0.1567$
Goodness-of-fit on F^2	1.003	0.605	1.106

purified by vapor diffusion of diethyl ether into an acetonitrile solution. They were all isolated as yellow crystals. Crystal data for **1a**, **1b**, and **2a** are given in Table 11. CCDC-224679 (for **1a**), -224680 (for **1b**) and -224681 (for **2a**) contain the supplementary crystallographic data for this paper. These data can be obtained free of charge from The Cambridge Crystallographic Data Centre via www.ccdc.cam.ac.uk/data_request/cif. [Cu(phen)(POP)]PF_6 was characterized by ^{1}H NMR and, IR spectroscopy, and elemental analysis.

[Cu(phen)(POP)]PF_6: $C_{48}H_{36}CuF_6N_2OP_3$: calcd. C 62.17, H 3.91, N 3.02; found C 62.08, H 3.99, N 2.92.

Instrumentation: The samples for photophysical studies were prepared by spin-coating a mixture of the Cu complex (20 wt.-%) and poly(methyl methacrylate) (80 wt.-%) in dichloromethane onto a glass slide. UV/Vis absorption and PL spectra were recorded on a Perkin–Elmer Lambda 35 UV/Vis spectrophotometer and a Perkin–Elmer LS50B fluorescence spectrophotometer, respectively. The ^{1}H NMR spectra were recorded on an AVANCZ 5000 spectrometer at 298 K, utilizing deuterated chloroform as the solvent and tetramethylsilane (TSM) as the standard. IR spectra were recorded on a Perkin–Elmer spectrophotometer in the 400–4000 cm^{-1} region, using a model RF-5301PC spectrophotometer.

Computational Methods: Calculations on the electronic ground-state of the investigated complexes were carried out at the B3LYP level of density functional theory, which has been proved very useful to calculate molecular orbital distributions for the interpretation of electrochemical and photochemical results for Ru^{II}[40] and square-planar Pt^{II} complexes.[41] B3LYP corresponds to the combination of Becke's three parameter exchange functional (B3) with the Lee–Yang–Parr for the correlation functional (LYP), using the LANL2DZ basis set that includes Dunning/Huzinaga valence double-ξ on the first row and Los Alamos ECP plus DZ on Na–Bi. The excited-state geometries were optimized at the CIS level of theory.[42,43] Time-dependent density functional theory (TDDFT) has recently become a reliable method for calculation of excited-state energies and has proven useful in the assignment of systems as complex as Ru^{II} and Cr^{III} polypyridyl complexes.[42−44] The nature of the low-lying excited states was explored using the time-dependent density functional theory (TDDFT) approach to derive both absorption spectra and emission spectra at the respective ground-state and excite-state geometries, which were compared to existed spectroscopic data. This B3LYP/LANL2DZ level of theory has proven useful for other transition metal systems. McCusker et al. have employed the B3LYP/LanL2DZ level of theory to study the excited-state electronic structures of $[RuL'_2(NCS)_2]^{4-}$ (where L′ = 4,4′-dicarboxylato-2,2′-bipyridine).[42] Adamo and colleagues[45] have presented a combined DFT//B3LYP and TDDFT study to predict the absorption spectra of $[Ru(bpy)(tpy)dmso]^{2+}$ (bpy = 2,2′-bipyridine, tpy = 2,2′:6′,2"-terpyridine; dmso = dimethyl sulfoxide). A double-ζ quality LANL2DZ basis was used for all atoms except oxygen and sulfur, which were described by 6-31G*. The results show good agreement between theory and experiment, with errors within 0.2 eV corresponding to the lowest allowed transition. Hay[46] has well reproduced the low-lying excited electronic states in the Ir^{III} complex $Ir(ppy)_3$ and related complexes using the B3LYP functional. "Double-ζ" quality basis sets were employed for the ligands (6-31G) and the Ir(LANL2DZ). The nature of the excited states, as well as the positive and negative ions with regard to "electron-hole" creation, is relevant to their use in OLED materials. In all computations no constraints were imposed on the geometry. All calculations are performed with the Gaussian 03 program suite. The molecular orbitals were visualized with MOLDEN 3.9.[47] Moreover, the qualitative concepts and the graphs derived from the Chem3D program suite highlight the basic interactions resulting from the DFT calculations.

Acknowledgments

This work was supported by the Major State Basis Research Development Program (no. 2002CB 613406), the National Nature Science Foundation of China (no. 90101026), and the Key Laboratory for Supramolecular Structure and Material of Jilin University.

[1] A. P. de Silva, D. B. Fox, T. S. Moody, S. M. Weir, *Pure Appl. Chem.* **2001**, *73*, 503–511.
[2] C. M. Rudzinski, D. G. Nocera, *Mol. Supramol. Photochem.* **2001**, *7*, 1–3.
[3] C. M. Elliott, F. Pichot, C. J. Bloom, L. S. Rider, *J. Am. Chem. Soc.* **1998**, *120*, 6781–6784.
[4] Y. D. Zhao, A. Richman, C. Storey, N. B. Radford, P. Pantano, *Anal. Chem.* **1999**, *71*, 3887–3893.
[5] K. E. Erkkila, D. T. Odom, J. K. Barton, *Chem. Rev.* **1999**, *99*, 2777–2796.
[6] L. Prodi, F. Bolletta, M. Montaltri, N. Zaccheroni, *Coord. Chem. Rev.* **2000**, *205*, 59–83.
[7] H. Ali, J. E. van Lier, *Chem. Rev.* **1999**, *99*, 2379–2450.
[8] C. A. Bignozzi, R. Argazzi, C. J. Kleverlaan, *Chem. Soc. Rev.* **2000**, *29*, 87–96.
[9] A. Juris, V. Balzani, F. Barigelletti, S. Campagna, P. Belser, A. von Zelewsky, *Coord. Chem. Rev.* **1988**, *84*, 85–98.
[10] D. R. McMillin, K. M. McNett, *Chem. Rev.* **1998**, *98*, 1201–1220.
[11] N. Armaroli, *Chem. Soc. Rev.* **2001**, *30*,113–124.
[12] D. V. Scaltrito, D. W. Thompson, J. A. O'Callaghan, G. J. Meyer, *Coord. Chem. Rev.* **2000**, *208*, 243–266.
[13] Q. S. Zhang, Q. G. Zhou, Y. X. Cheng, L. X. Wang, D. G. Ma, X. B. Jing, *Adv. Mater.* **2004**, *16*, 432–436.
[14] M. K. Eggleston, D. R. McMillin, K. S. Koenig, A. J. Pallenberg, *Inorg. Chem.* **1997**, *36*, 172–173.
[15] C. T. Cunningham, K. L. H. Cunningham, J. F. Michalec, D. R. McMillin, *Inorg. Chem.* **1999**, *38*, 4388–4392.
[16] R. A. Rader, D. McMillin, M. T. Buckner, T. G. Matthews, D. J. Casadonte, R. K. Lengel, S. B. Whittaker, L. M. Darmon, F. E. Lytle, *J. Am. Chem. Soc.* **1981**, *103*, 5906–5912.
[17] P. A. Breddels, P. A. M. Berdowski, G. Blasse, *J. Chem. Soc., Faraday Trans. 2* **1982**, *78*, 595–599.
[18] C. E. A. Palmer, D. R. McMillin, *Inorg. Chem.* **1987**, *26*, 3837–3840.
[19] M. Kranenburg, Y. E. M. van der Burgt, P. C. J. Kamer, P. W. N. M. van Leeuwen, K. Goubitz, J. Fraanje, *Organometallics* **1995**, *14*, 3081–3089.
[20] W. Koch, M. C. Holthausen, *A Chemist's Guide to Density Functional Theory*; Wiley-VCH, Weinheim, Germany, **2000**.
[21] C. Adamo, B. V. di Matteo, *Adv. Quantum Chem.* **1999**, *36*,4–7.
[22] R. Bauernschmitt, R. Ahlrichs, *Chem. Phys. Lett.* **1996**, *256*, 454–464.
[23] F. Furche, *J. Chem. Phys.* **2001**, *114*, 5982–5992.
[24] G. Ricciardi, A. Rosa, E. J. Baerends, *J. Phys. Chem. A* **2001**, *105*, 5242–5454.
[25] F. Furche, R. Ahlrichs, A. Sobanski, F. Vögtle, C. Wachsman, E. Weber, S. Grimme, *J. Am. Chem. Soc.* **2000**, *122*, 1717–1724.
[26] P. Aslanidis, P. J. Cox, S. Divanidis, A. C. Tsipis, *Inorg. Chem.* **2002**, *41*, 6875–6886.
[27] Z. A. Siddique, Y. Yamamoto, T. Ohno, K. Nozaki, *Inorg. Chem.* **2003**, *42*, 6366–6378.
[28] S. Fantacci, F. D. Angelis, A. Selloni, *J. Am. Chem. Soc.* **2003**, *125*, 4381–4387.
[29] O. Gritsenko, E. J. Baerends, *J. Chem. Phys.* **2004**, *121*, 655–661.
[30] A. Dreuw, M. Head-Gordon, *J. Am. Chem. Soc.* **2004**, *126*, 4007–4016.
[31] M. Turki, C. Daniel, S. Záliš, A. Vlèek, Jr., J. van Slageren, D. Stufkens, *J. Am. Chem. Soc.* **2001**, *123*, 11431–11440.
[32] A. Gabrielsson, S. Záliš, P. Matousek, M. Towrie, A. Vlèek, Jr., *Inorg. Chem.* **2004**, *43*, 7380–7388.
[33] S. Záliš, N. Ben Amor, C. Daniel, *Inorg. Chem.* **2004**, *43*, in press.
[34] J. F. Brière, M. Côté, *J. Phys. Chem. B* **2004**, *108*, 3123–3129.
[35] S. Grimme, M. Parac, *ChemPhysChem* **2003**, *4*, 292–295.
[36] H. X. Zhang L. Yang, A. M. Ren, J. K. Feng, X. D. Liu, Y. G. Ma, *Inorg. Chem.* **2004**, *43*, 5961–5972.
[37] L. Yang, A. M. Ren, J. K. Feng, Y. G. Ma, M. Zhang, X. D. Liu, J. C. Shen, H. X. Zhang, *J. Phys. Chem.* **2004**, *108*, 6797–6808.
[38] S. M. Kuang, D. G. Guttell, D. R. McMillin, P. E. Fanwichk, R. A. Walton, *Inorg. Chem.* **2002**, *41*, 3313–3322.
[39] D. G. Cuttell, S. M. Kuang, P. E. Fanwick, D. R. McMillin, D. A. Walton, *J. Am. Chem. Soc.* **2002**, *124*, 6–7.
[40] K. A. Nguyen, J. Kennel, R. Pachter *J. Chem. Phys.* **2002**, *117*, 7128–7136.
[41] S. R. Stoyanov, J. M. Villegas, D. P. Rillema, *Inorg. Chem.* **2003**, *42*, 7852–7860.
[44] J. E. Monat, J. H. Rodriguez, J. K. McCusker, *J. Phys. Chem. A* **2002**, *106*, 7399–7406.
[45] J. H. Rodrigues, D. E. Wheeler, J. K. McCusker, *J. Am. Chem. Soc.* **1998**, *120*, 12051–12068.
[46] K. Zheng, J. Wang, W. Peng, X. Liu, F. Yun, *J. Phys. Chem. A* **2001**, *105*, 10 899–10 905.
[47] H. Ciofini, C. A. Daul, C. Adamo, *J. Phys. Chem. A* **2003**, *107*, 11190–11194.
[48] H. P. Jeffrey, *J. Phys. Chem. A* **2002**, *106*, 1634–1641.
[49] G. Schaftenaar, CAOS/CAMM Center Nijmegen Toernooiveld, Nijmegen, The Netherlands, **1991**.

Received: November 09, 2004

